

Radiative Characteristics of Deep Convective Systems in the Tropical Western Pacific

M. P. Jensen

Columbia University

Department of Applied Physics and Applied Mathematics

National Aeronautics and Space Administration

Goddard Institute for Space Studies

New York, New York

Introduction

Deep convection and its associated anvil outflow cause a large perturbation in the radiation budget by increasing the shortwave (SW) albedo and reducing the infrared emission to space over time scales of one to several days and spatial scales on the order of the size of a general circulation model (GCM) grid box. These cloud systems impact the local radiative heating profile through solar heating near cloud-top and infrared (IR) heating/cooling at cloud-base/top. They also cause a large surface solar and IR cloud forcing.

Methods and Analysis

The radiative characteristics of several deep convective cases over Manus are investigated. Data from the Atmospheric Radiation Measurement (ARM) Program Tropical Western Pacific (TWP) site at Manus is combined with satellite data from the ARM external center and the Tropical Rainfall Measuring Mission (TRMM) satellite to describe the three-dimensional (3D) structure of the ice and liquid water content (I/LWC) in the precipitating regions of each system.

To describe the 3D-I/LWC structure of the deep convective system we use the radar reflectivity from the TRMM Precipitation Radar (PR) along with an appropriate Z-I/LWC parameterization assuming that the hydrometeor population obeys a log-normal distribution. For heights below the freezing level, we employ a parameterization based on the Marshall-Palmer (1948) distribution with $LWC = 0.004Ze^{0.55}$ and a mean diameter of $D_m = 1500 \mu\text{m}$. When the height is greater than the freezing level, two separate regimes are parameterized. For PR radar reflectivity $\text{dBZe} < 29$, $IWC = 0.001Zi^{0.96}$ with $D_m = 200 \mu\text{m}$ and for $\text{dBZe} \geq 29$ an upper limit of 2.5 gm^{-3} is used. These parameterizations were derived for island-based deep convection during the Maritime Continent Thunderstorm Experiment (MCTEX) (Jensen 2000). The TRMM PR is not sensitive enough to detect small cloud particles. To account for small cloud particles near the top of the anvil complex, we assume a layer of small particles with a mean radius of $20 \mu\text{m}$ and an ice water content (IWC) of 0.08 gm^{-3} (Knollenberg et al. 1993) between the top of the radar echo and the IR equivalent cloud-top height from Geostationary Meteorological Satellite (GMS) IR brightness temperature measurements. The resulting 3D representation of the cloud microphysics is then used as input to a two-stream radiative transfer model (Toon et al. 1989). This

model uses Mie scattering theory to calculate scattering by cloud and precipitation particles and a correlated-k technique for absorption by atmospheric constituents (Kato et al. 1999) for 26 bands in the solar spectrum from 0.25 to 4.5 μm and 18 bands in the infrared from 4.8 to 35.8 μm . The profiles of temperature and water vapor are taken from a sounding preceding the TRMM overflight time. An independent pixel approximation (IPA) (Cahalan et al. 1994) is used for the radiative transfer calculations, i.e., we treat each column individually as plane-parallel and homogeneous in each of 85 layers, neglecting interactions between columns.

Figure 1 shows a comparison of the top-of-atmosphere (TOA) modeled broadband SW and longwave (LW) fluxes and measurements from the Cloud and Earth Radiant Energy System (CERES) aboard the TRMM satellite. This comparison shows that for SW fluxes, in the precipitating regions of the cloud, the measured and modeled fluxes agree to better than 20% with a mean of 7.7%. For LW fluxes this agreement is slightly better with a mean of 3.6%. Some large discrepancies are seen near cloud and precipitation region edges, where the IPA breaks down, and differences in CERES and TRMM resolution result in poor comparisons. This agreement to within 20% is consistent with previous studies (Jensen 2000) of deep convective systems during the MCTEX. Because we have concentrated on cases over the Manus ARM TWP site, we can also compare modeled and measured fluxes at the surface. Figure 2 shows the difference between the modeled and measured solar cloud forcing at the surface for 18 different cases where the TRMM PR observed precipitation over Manus. For > 85% of the cases the modeled SW cloud forcing at the surface agrees with the measured SW cloud forcing to within 20%. The few outliers represent cases where Manus was near the edge of a precipitating region, and the large differences probably occur as a result of a breakdown in the IPA.

To test the sensitivity of our results to the parameters in the set of Z-I/LWC relations, we compare the modeled TOA upwelling fluxes to those measured by the CERES instrument for a set of 17 different combinations of parameterizations and assumptions for the IWC. Table 1 summarizes the different parameterizations used in the cloud-top and cloud regimes for each run. The range of IWC and particle sizes for the cloud-top small particle regime (IR equivalent cloud-top height $> Z >$ radar each height) are taken from in situ measurements made by Knollenberg et al. (1993) near the tops of deep anvil systems during the Stratosphere-Troposphere Exchange Project (STEP (0.08 gm^{-3})) and in situ measurements reported by McFarquhar and Heymsfield (1997) from the Central Equatorial Pacific Experiment (CEPEX) (0.004 gm^{-3}). The range of parameters for the Z-IWC relationships in the precipitating regions of the anvil system ($Z >$ freezing level and $\text{dBZe} < 29$) represent conservative bounds to the regression fits of Z_i versus IWC from Jensen (2000) for island-based tropical anvil systems observed during MCTEX. Figure 3 shows the mean differences (\pm one standard deviation) between the modeled and measured fluxes for each of 17 different variations of the IWC description. These results show that the reflected solar flux is not very sensitive to changes in the number of large precipitation particles above, or below, the freezing level. Rather, these fluxes are most sensitive to changes in the size and number concentration of the small ice crystals near the top of the cloud. This sensitivity analysis shows that the modeled TOA upwelling fluxes are not very sensitive to changes in the parameters of the Z-IWC relationships in the precipitating regions of the system. These modeled fluxes are, however, very sensitive to differences in the IWC and mean particle sizes in the cloud-top, small particle regions of the cloud.

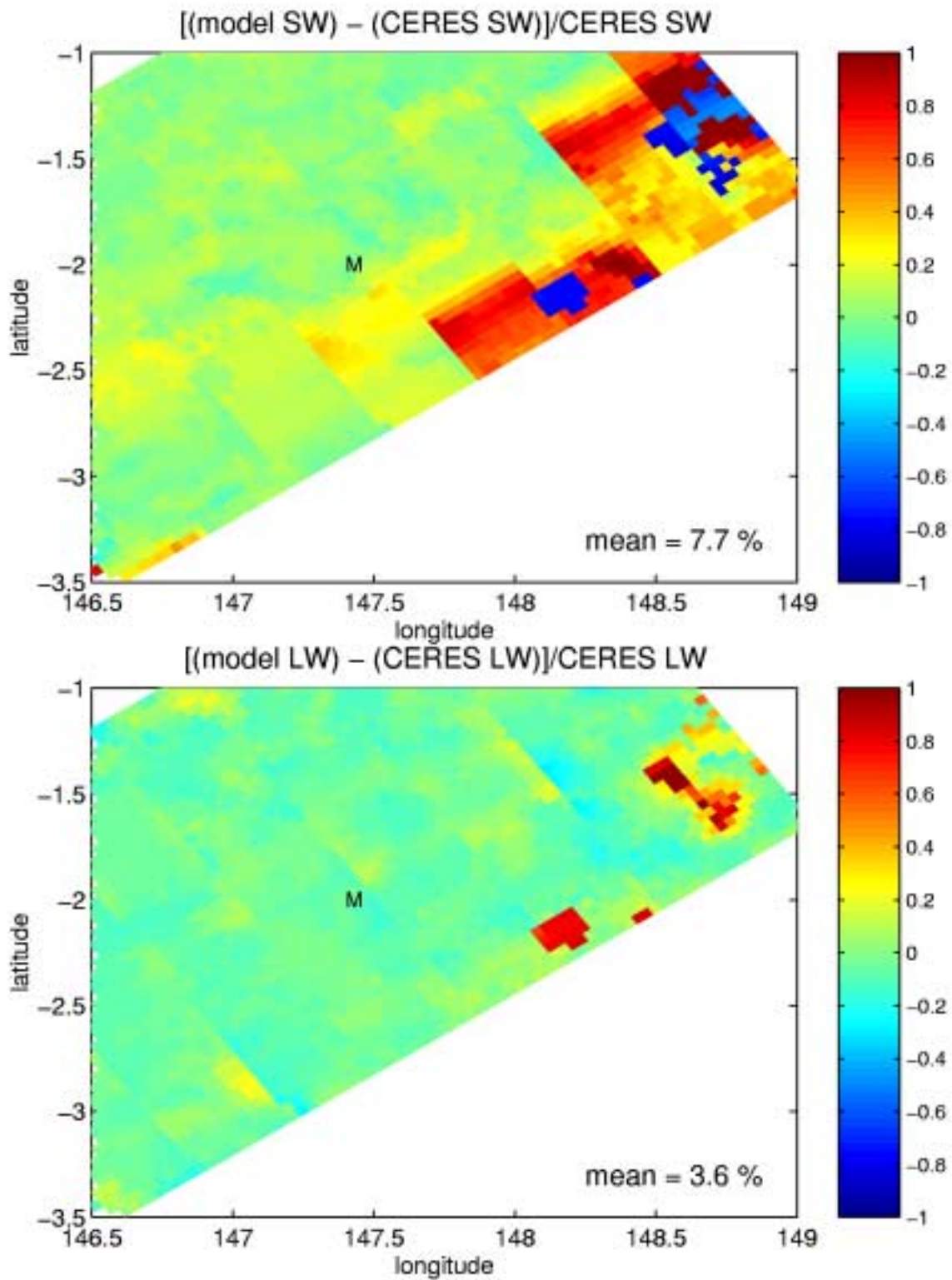


Figure 1. Relative difference between the TOA modeled broadband SW (top) and LW (bottom) fluxes and measurements from the CERES instrument aboard the TRMM satellite.

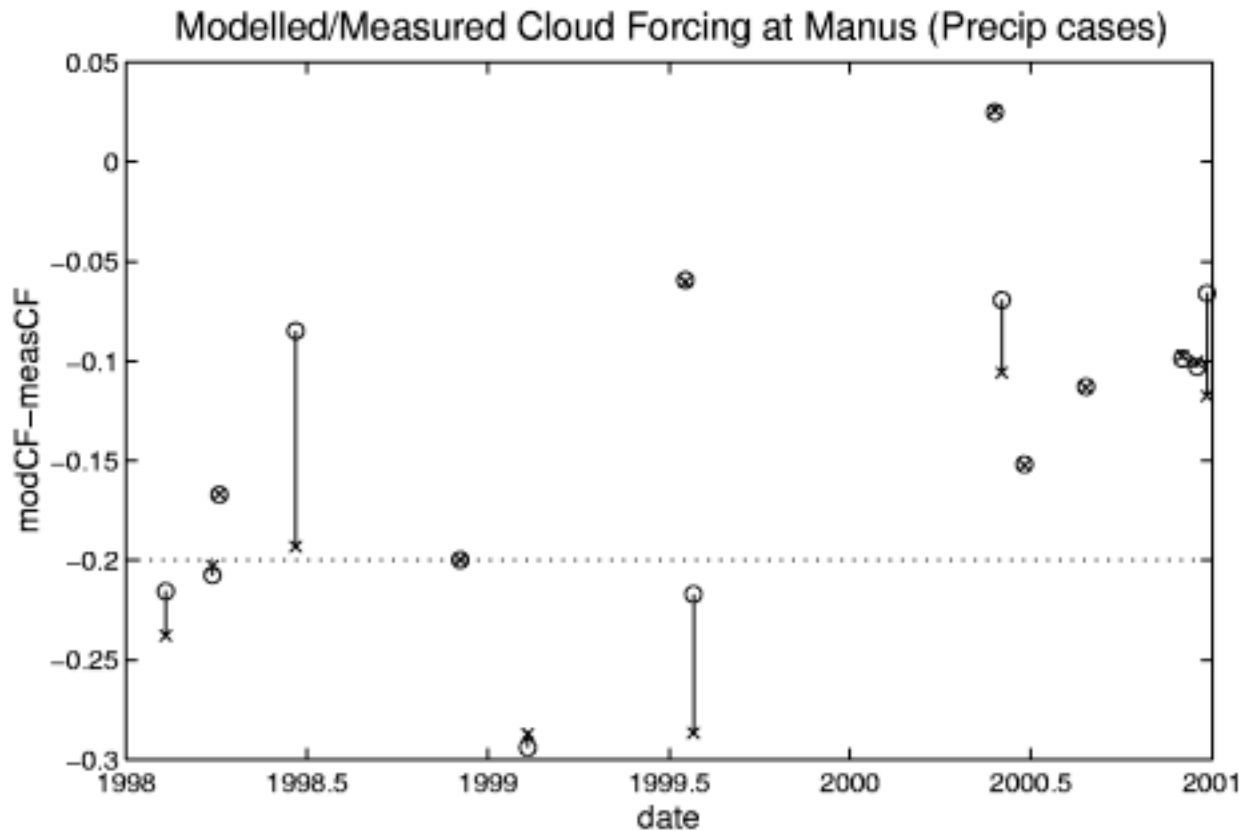


Figure 2. Comparison of the modeled and measured normalized SW cloud forcing (Normalized CF = [(clear-sky flux)-(mod/measflux)]/(clear_sky flux)) at the surface for Manus Island. Cloud heterogeneity is addressed by comparing to the 1-minute downwelling solar flux (X) and the 10-minute mean of the downwelling solar flux (O). Only cases where precipitation was detected by the TRMM PR are included.

Conclusions

We are able to model the TOA and surface broadband radiative fluxes to within 20% of the values observed by CERES over the precipitating regions of deep convective systems using a dataset that is collected over the entire tropics. These modeled fluxes are rather sensitive to the choice of IWC in the small particle regime near cloud-top and relatively insensitive to the parameters of the Z-IWC relationships describing the large particle regime in the precipitating regions of the cloud. Deep convective clouds and their associated anvil systems represent 20 to 30% of the total cloud fraction in the TWP and represent a large perturbation on the vertical distribution of radiative heating in the atmospheric column. Therefore, an understanding of the radiative impacts of these systems is important on climatic time scales.

Table 1. Summary of the different parameterizations used in the cloud-top (column 2) and the cloud (column 3) regimes for the model runs shown in Figure 3.		
Run #	IRTb height > Z > radar echo top	Z > freezing lev & dBZE < 29
1	IWC=0.08 gm ⁻³ , D _m =20μm	IWC=0.001Z ^{0.96} , D _m =200μm
2	IWC=0.004 gm⁻³ , D _m =20μm	IWC=0.001Z ^{0.96} , D _m =200μm
3	IWC=0.08 gm ⁻³ , D_m=50μm	IWC=0.001Z ^{0.96} , D _m =200μm
4	IWC=0.08 gm ⁻³ , D _m =20μm	IWC= 0.0025 Z ^{0.96} , D _m =200μm
5	IWC=0.08 gm ⁻³ , D _m =20μm	IWC= 0.003 Z ^{0.96} , D _m =200μm
6	IWC=0.08 gm ⁻³ , D _m =20μm	IWC=0.001Z ^{0.36} , D _m =200μm
7	IWC=0.08 gm ⁻³ , D _m =20μm	IWC=0.001Z ^{0.25} , D _m =200μm
8	IWC=0.08 gm ⁻³ , D _m =20μm	IWC=0.001Z ^{1.25} , D _m =200μm
9	IWC=0.08 gm ⁻³ , D _m =20μm	0, 0
10	IWC=0.004 gm⁻³ , D _m =20μm	0, 0
11	0, 0	IWC=0.001Z ^{0.96} , D _m =200μm
12	IWC=0.1 gm⁻³ , D _m =20μm	IWC=0.001Z ^{0.96} , D _m =200μm
13	IWC=0.6 gm⁻³ , D _m =20μm	IWC=0.001Z ^{0.96} , D _m =200μm
		Z < freezing lev
14	IWC=0.08 gm ⁻³ , D _m =20μm	LWC= 0.002 Z ^{0.55}
15	IWC=0.08 gm ⁻³ , D _m =20μm	LWC= 0.006 Z ^{0.55}
16	IWC=0.08 gm ⁻³ , D _m =20μm	LWC=0.004Z ^{0.45}
17	IWC=0.08 gm ⁻³ , D _m =20μm	LWC=0.004Z ^{0.65}

Corresponding Author

M. P. Jensen, mjensen@giss.nasa.gov, (212) 678-6038

References

Cahalan, R. F., W. Ridgeway, W. J. Wiscombe, T. L. Bell, and J. B. Snider, 1994: The albedo of fractal stratocumulus clouds. *J. Atmos. Sci.*, **51**, 2434-2455.

Jensen, M. P., 2000: "Lifecycles and Radiative Impacts of Anvil Cirrus Outflow During the Maritime Continent Thunderstorm Experiment," PhD dissertation, p. 94, Pennsylvania State University.

Kato, S., T. P. Ackerman, J. H. Mather, and E. E. Clothiaux, 1999: The k-distribution method and correlated-k approximation for a shortwave radiative transfer model. *J. Quant. Spec. Rad. Tran.*, **62**, 109-121.

Knollenberg, R. G., K. Kelly, and J. C. Wilson, 1993: Measurements of high number densities of ice crystals near the tops of tropical cumulonimbus. *J. Geophys. Res.*, **98**, 8639-8664.

Marshall, J. S., and W. M. Palmer, 1948: The distribution of raindrops with size. *J. Meteor.*, **5**, 165-166.

McFarquhar, G. M., and A. J. Heymsfield, 1997: Parameterization of tropical cirrus ice crystal size distributions and implications for radiative transfer: Results from CEPEX. *J. Atmos. Sci.*, **54**, 2187-2200.

Toon, O. B., C. P. McKay, T. P. Ackerman, and K. Santhanam, 1989: Rapid calculation of radiative heating rates and photodissociation rates in inhomogeneous multiple scattering atmospheres. *J. Geophys. Res.*, **94**, 16,287-16,301.

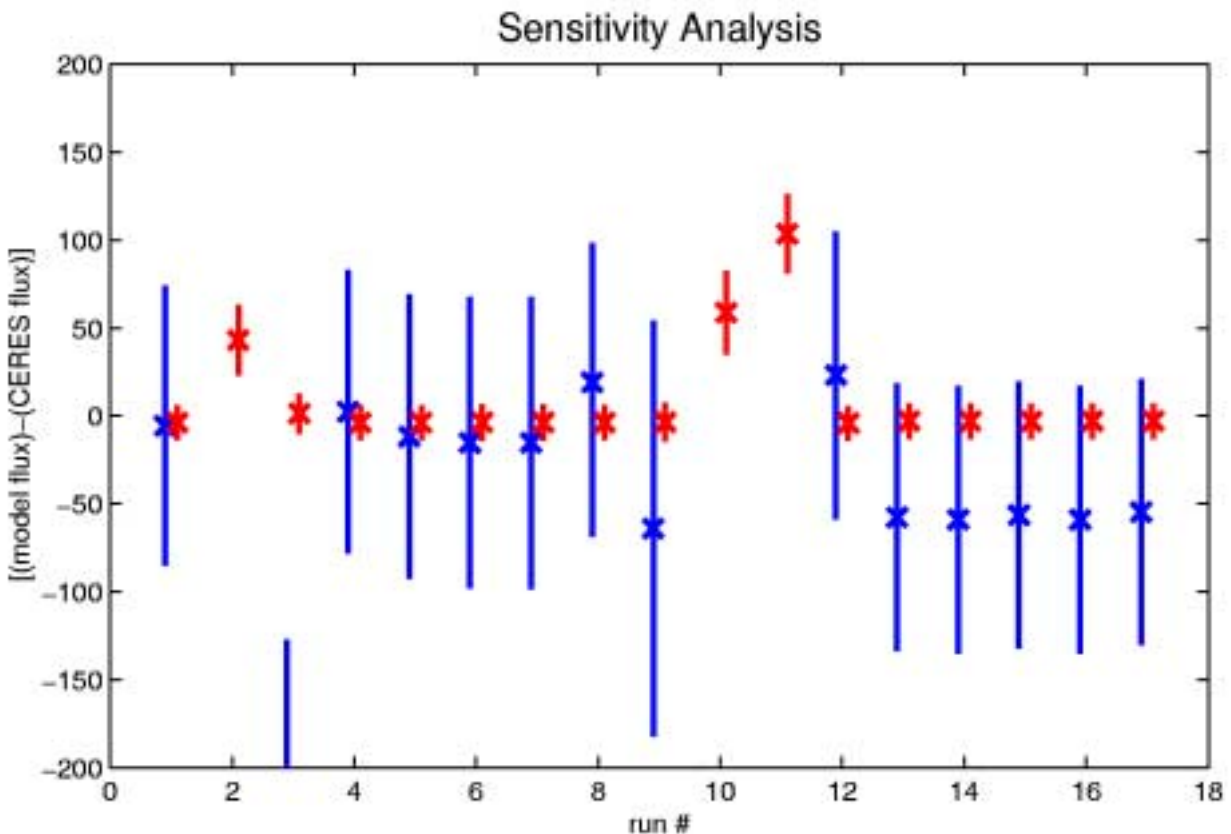


Figure 3. Modeled TOA upwelling flux – CERES measured TOA upwelling flux (solar = blue, IR = red) for a set of 17 different combinations of parameterizations and assumptions for ice water content. The X represents the mean of this difference over all raining pixels, the bar represents plus/minus one standard deviation.